Supporting Information

Three-dimensional Microspheres Constructed by MoS_2 Nanosheets Supported on Multiwalled Carbon Nanotubes for Optimized Sodium Storage

*Lei Chen[1], Mao Shen[1], Shi-Bin Ren[*1], Yu-Xiang Chen[1], Wei Li [1], and De-Man Han[**1]*

[1] School of Pharmaceutical Chemical and Materials Engineering, Taizhou University,

Taizhou, 318000, P. R. China

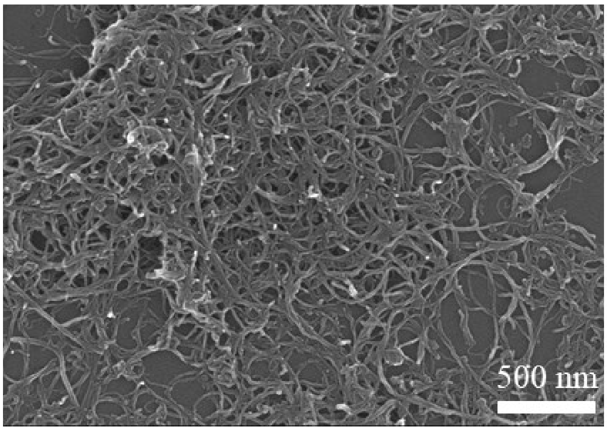

Figure S1. The SEM image of MWCNTs.

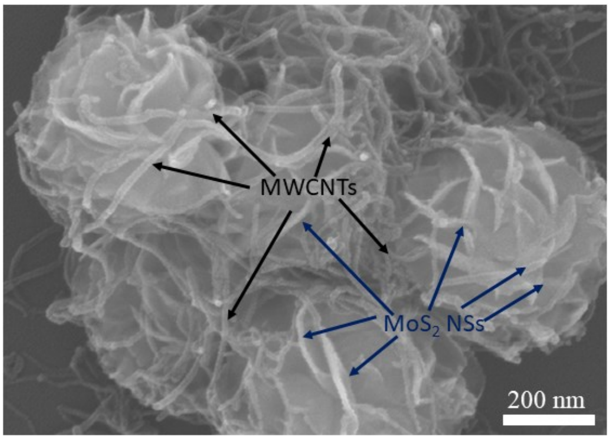

Figure S2. SEM images of MoS_2-MSs/MWCNTs.

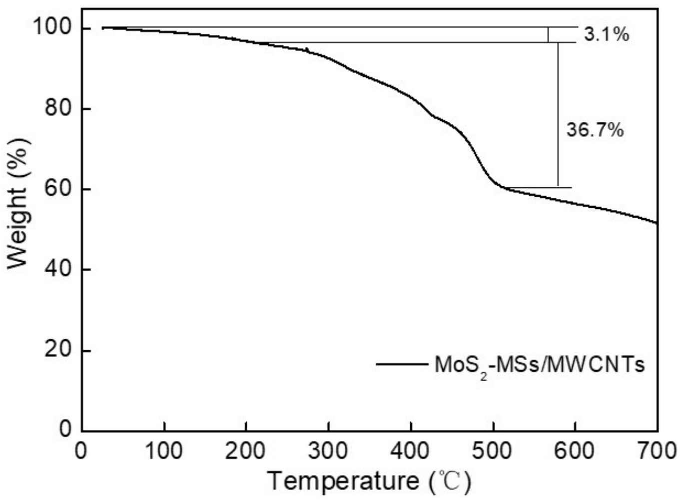

Figure S3. Thermal gravimetric curve of MoS_2-MSs/MWCNTs composite.

Here, MoS_2 was oxidized to MoO_3 completely and MWCNTs were oxidized to CO_2. Therefore, the MoS_2 content in the composite could be calculated to be about 69.1 wt%, according to the previously reported literatures.

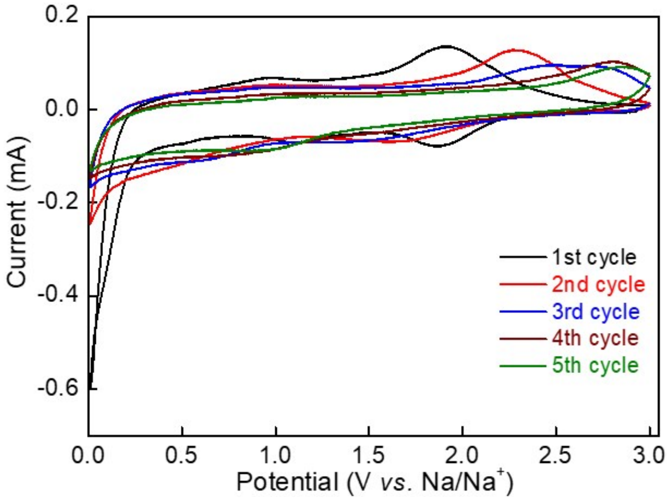

Figure S4. CV curves of the initial five cycles for MoS_2-MSs at 0.1 mV s^{-1} within 0.01 and 3.0 V (V *vs.* Na/Na^+).

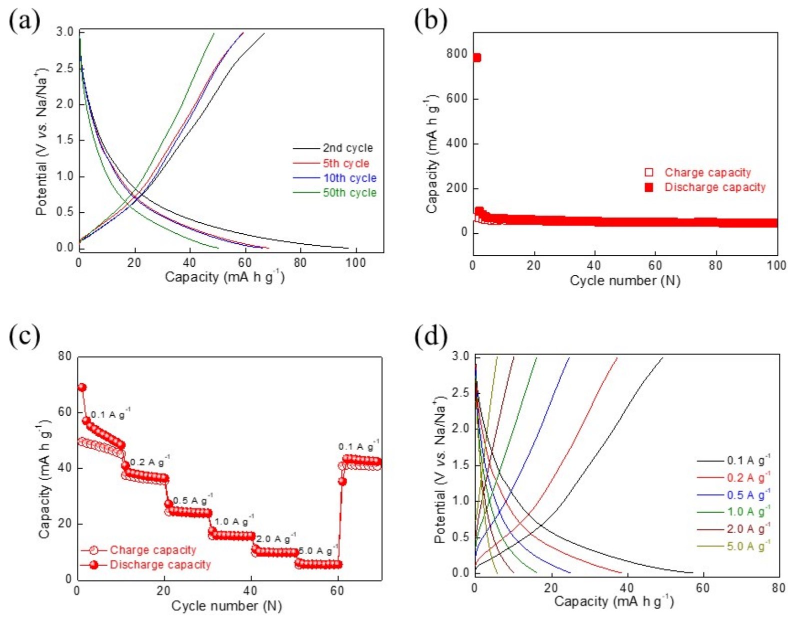

Figure S5. Electrochemical performance of MWCNTs electrodes in the voltage window 0.01-3.0 V (V *vs.* Na/Na^+): (a) Galvanostatic discharge/charge profiles of 2^{nd}, 5^{th}, 10^{th}, 50^{th} cycles at a current density of 0.1A g^{-1}; (b) Cycling performance at 0.1A g^{-1} over 100 cycles; (c) Rate capability at different current densities of 0.1, 0.2, 0.5, 1.0, 2.0 and 5.0 A g^{-1}; (d) the charge-discharge curves at the various current densities.

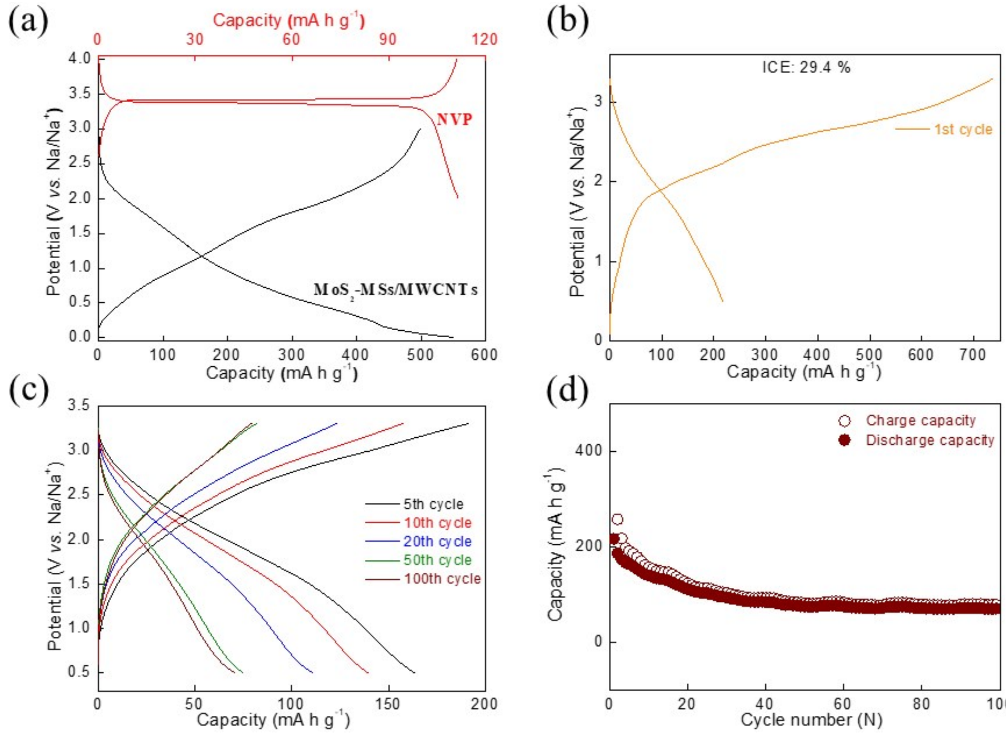

Figure S6. Electrochemical performances of MoS_2-MSs/MWCNTs || $Na_3V_2(PO_4)_3$ full cell: (a) The Charge-discharge curves of Na||$Na_3V_2(PO_4)_3$ and Na||MoS_2-MSs/MWCNTs half batteries; (b) the first GCD curve at 0.1 A g^{-1} in the voltage range of 0.5-3.3 V; (C) discharge/charge profiles of 5^{th}, 10^{th}, 20^{th}, 50^{th}, 100^{th} cycles at 0.1A g^{-1}; (d) cycling performance at 0.1 A g^{-1} for 100 cycles.

The MoS_2-MSs/MWCNTs||$Na_3V_2(PO_4)_3$ full cell was assembled by using MoS_2-MSs/MWCNTs and $Na_3V_2(PO_4)_3$ as the anode and cathode, respectively. The current density and capacity of the full cell are based on the anode mass. **Figure S5b** shown the first charge and discharge specific capacities of full-cell were 737.03 and 216.68 mA h g^{-1}, respectively, with a low Coulombic efficiency of 29.4 %. The obviously irreversible capacity is mainly attributed to the formation of the SEI layer [S1, S13]. After 100 cycles, the full cell delivers a discharge capacity of 70.96 mA h g^{-1} (**Figure S5d**).

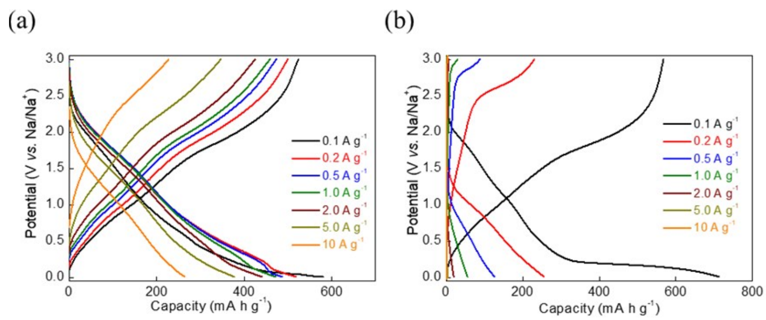

Figure S7. discharging-charging profiles of MoS_2-MSs/MWCNTs (a) and MoS_2-MSs (b) at various specific currents.

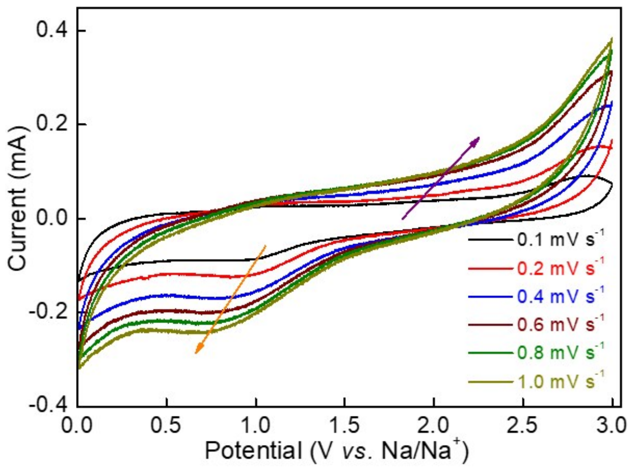

Figure S8. CV curves of MoS_2-MSs at various scan rates from 0.1 to 1.0 mV s^{-1}.

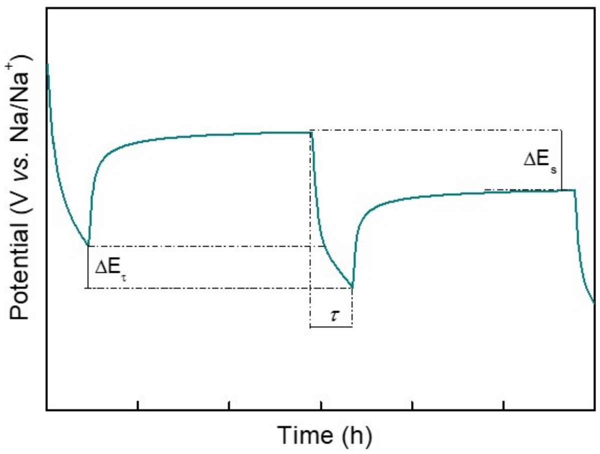

Figure S9. A single step of a GITT experiment.

The D_{Na+} could be calculated using the formula:

$$D_{Na^+} = \frac{4}{\pi\tau}\left(\frac{m_B V_M}{M_B A}\right)^2\left(\frac{\Delta E_s}{\Delta E_\tau}\right)^2$$

Where τ represents the constant current pulse time; m_B, M_B, and V_M are the mass, molar weight, and molar volume of the active materials, respectively. A is the total contact area between the electrolyte and the electrode. ΔE_s and ΔE_τ are the changes in steady-state voltage after subtracting the IR drop and the total transient change in cell voltage during a single titration (**Figure S8**).

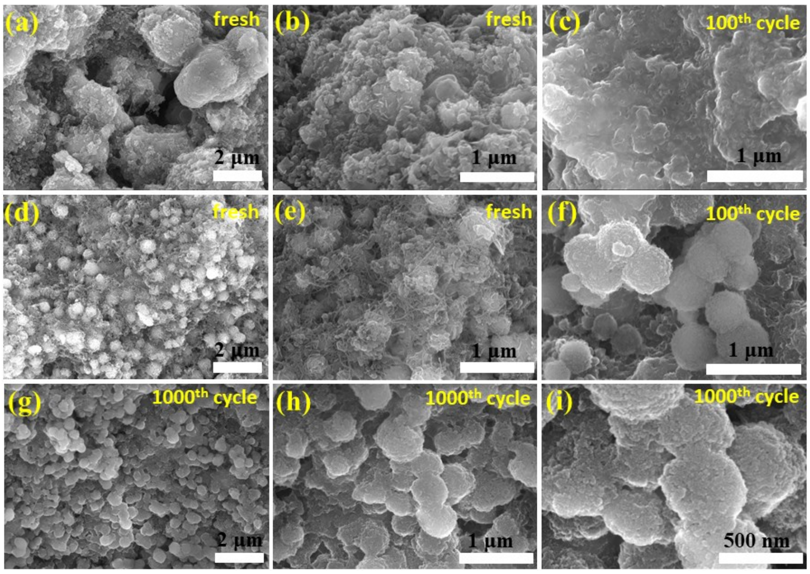

Figure S10. SEM images of MoS_2-MSs before cycling (a & b); after 100 cycles at 0.1 A g^{-1} (c); MoS_2-MSs/MWCNTs before cycling (d & e); after 100 cycles at 0.1 A g^{-1} (f); after 1000 cycles at 2.0 A g^{-1} (g-i).

Table S1. Comparison of the electrochemical performance of MoS_2-MSs/MWCNTs composite with previously reported MoS_2-based anode for SIBs.

Samples	**Capacity (mA h g^{-1})**	**Retention**	**Rate property (mA h g^{-1})**	**Ref.**
N-doped MoS_2/C	599.7 mA h g^{-1} at 0.1 A g^{-1}	83.4 % (50 cycles)	242 mA h g^{-1} at 5 A g^{-1}	**S2**
S/MoS_2 architectures	497.6 mA h g^{-1} at 0.1 A g^{-1}	83.0 % (100 cycles)	243.3 mA h g^{-1} at 2 A g^{-1}	**36**
MoS_2/NCF-MP	471.8 mA h g^{-1} at 0.1 A g^{-1}	101.7 % (100 cycles)	217 mA h g^{-1} at 30 A g^{-1}	**37**
tulip-MoS_2/NG	320 mA h g^{-1} at 0.1 A g^{-1}	99.4 % (100 cycles)	216 mA h g^{-1} at 5 A g^{-1}	**39**
MoS_2@CF	343 mA h g^{-1} at 0.1 A g^{-1}	104.9 % (100 cycles)	171 mA h g^{-1} at 5 A g^{-1}	**40**
MoS_2/CNTs	495.9 mA h g^{-1} at 0.2 A g^{-1}	84.8 % (80 cycles)	328.4 mA h g^{-1} at 0.5 A g^{-1}	**41**
graphene@MoS_2@C	604 mA h g^{-1}	86.1 %	304 mA h g^{-1}	**S3**

	at 0.1 A g^{-1}	(110 cycles)	at 5 A g^{-1}	
MoS_2/PDC	475 mA h g^{-1} at 0.2 A g^{-1}	85.6 % (340 cycles)	301.5 mA h g^{-1} at 5 A g^{-1}	**S4**
MoS_2@C-CMC	352 mA h g^{-1} at 0.08 A g^{-1}	81.2 % (100 cycles)	205 mA h g^{-1} at 1 A g^{-1}	**S5**
MoS_2 nanosheets /Carbon Fibers	362 mA h g^{-1} at 0.1 A g^{-1}	91.2 % (100 cycles)	225 mA h g^{-1} at 1 A g^{-1}	**S6**
MoS_2-reduced graphene oxide (rGO)	345 mA h g^{-1} at 0.1 A g^{-1}	88.4 % (50 cycles)	245 mA h g^{-1} at 1 A g^{-1}	**S7**
MoS_2/C-MWCNT	617 mA h g^{-1} at 0.2 A g^{-1}	83.9 % (300 cycles)	324 mA h g^{-1} at 20 A g^{-1}	**45**
Nervous-like MoS_2/MWCNT	571 mA h g^{-1} at 0.1 A g^{-1}	92.4 % (110 cycles)	411 mA h g^{-1} at 2 A g^{-1}	**46**
Graphene-Wrapped MoS_2 (MoS_2-G)	495.1 mA h g^{-1} at 0.2 A g^{-1}	82.5 % (100 cycles)	345 mA h g^{-1} at 1.6 A g^{-1}	**S8**
MoS_2-rGO/HCS	635 mA h g^{-1} at 0.1 A g^{-1}	86.9 % (100 cycles)	364 mA h g^{-1} at 5 A g^{-1}	**S9**
MoS_2@C nanotube composite	640 mA h g^{-1} at 0.5 C	80 % (200 cycles)	370 mA h g^{-1} at 5 C	**S10**
MoS_2@C nanosheets @MoS_2 nanorods	477 mA h g^{-1} at 0.1 A g^{-1}	86.3 % (100 cycles)	284 mA h g^{-1} at 4 A g^{-1}	**S11**
CNT@NCT@W-MoS_2/C	530 mA h g^{-1} at 0.1 A g^{-1}	——	230 mA h g^{-1} at 2 A g^{-1}	**S12**
MoS_2-C nanosheets	383.4 mA h g^{-1} at 0.1 A g^{-1}	101.3 % (100 cycles)	275 mA h g^{-1} at 8 A g^{-1}	**S13**
N-MoS_2/C	649 mA h g^{-1} at 0.2 C	78 % (200 cycles)	387.9 mA h g^{-1} at 10 C	**S14**
1T-MoS_2/CC arrays	768 mA h g^{-1} at 0.2 A g^{-1}	80 % (200 cycles)	276 mA h g^{-1} at 2 A g^{-1}	**53**
MoS_2-MSs/MWCNTs composite	**550 mA h g^{-1} at 0.1 A g^{-1}**	**94.4 % (100 cycles)**	**227 mA h g^{-1} at 10 A g^{-1}**	**This work**

Table S2. The calculated values of SEI layer resistance (R_{SEI}), charge-transfer resistance (R_{ct}), σ and sodium-ion diffusion coefficient (D_{Na+}) for both samples.

Samples	R_{SEI} (Ω)	R_{ct} (Ω)	σ	D_{Na+} (cm^2 s^{-1})
MoS_2-MSs	201.7	14.95	117.84	2.14×10^{-11}
MoS_2-MSs/MWCNTs	19.05	78.72	16.67	0.89×10^{-12}

References

[S1] N. Wang, Z. Bai, Y. Qian, J. Yang. Double-Walled Sb@TiO_{2-x} Nanotubes as a Superior High-Rate and Ultralong-Lifespan Anode Material for Na-Ion and Li-Ion

Batteries. *Adv. Mater.* **2016**, *28*, 4126-4133.

[S2] Y. S. Cai, H. L. Yang, J. Zhou, Z. G. Luo, G. Z. Fang, S. N. Liu, A. Q. Pan, S. Q. Liang. Nitrogen doped hollow MoS_2/C nanospheres as anode for long-life sodium-ion batteries. *Chem. Eng. J.* **2017**, *327*, 522-529.

[S3] Y. Q. Teng, H. L. Zhao, Z. J. Zhang, L. Zhao, Y. Zhang, Z. L. Li, Q. Xia, Z. H. Du, K. Swierczek. MoS_2 Nanosheets Vertically Grown On Reduced Graphene Oxide via Oxygen Bonds with Carbon Coating as Ultrafast Sodium Ion Batteries Anodes. *Carbon* **2017**, *119*, 91-100.

[S4] M. Lin, M. Deng, C. Zhou, Y. Shu, L. Yang, L. Ouyang, Q. Gao, M. Zhu. Popcorn derived carbon enhances the cyclic stability of MoS_2 as an anode material for sodium-ion batteries. *Electrochim. Acta* **2019**, *309*, 25-33.

[S5] X. Xie, T. Makaryan, M. Zhao, K. L. V. Aken, Y. Gogotsi, G. Wang. MoS_2 Nanosheets Vertically Aligned on Carbon Paper: A Freestanding Electrode for Highly Reversible Sodium-Ion Batteries. *Adv. Energy Mater.* **2016**, *6*, 1502161.

[S6] Y. Zhang, H. Tao, T. Li, S. Du, J. Li, Y. Zhang, X. Yang. Vertically Oxygen-Incorporated MoS_2 Nanosheets Coated on Carbon Fibers for Sodium-Ion Batteries. *ACS Appl. Mater. Interfaces* **2018**, *10*, 35206-35215.

[S7] W. Qin, T. Chen, L. Pan, L. Niu, B. Hu, D. Li, J. Li, Z. Sun. MoS_2-reduced graphene oxide composites via microwave assisted synthesis for sodium ion battery anode with improved capacity and cycling performance. *Electrochim. Acta* **2015**, *153*, 55-61.

[S8] S. Anwer, Y. Huang, B. Li, B. Govindan, K. Liao, W. J. Cantwell, F. Wu, R. Chen, L. Zheng. Nature-Inspired, Graphene-Wrapped 3D MoS_2 Ultrathin Microflower Architecture as a High-Performance Anode Material for Sodium-Ion Batteries. *ACS Appl. Mater. Interfaces* **2019**, *11*, 22323-22331.

[S9] X. Hu, Y. Li, G. Zeng, J. Jia, H. Zhan, Z. Wen. Three-Dimensional Network Architecture with Hybrid Nanocarbon Composites Supporting Few-Layer MoS_2 for Lithium and Sodium Storage. *ACS Nano* **2018**, *12*, 1592-1602.

[S10] X. Zhang, X. Li, J. Liang, Y. Zhu, Y. Qian. Synthesis of MoS_2@C Nanotubes Via the Kirkendall Effect with Enhanced Electrochemical Performance for Lithium Ion and Sodium Ion Batteries. *Small* **2016**, *12*, 2484-2491.

[S11] G. K. Veerasubramani, M.-S. Park, G. Nagaraju, D.-W. Kim. Unraveling the Na-ion storage performance of a vertically aligned interlayer-expanded two-dimensional MoS_2@C@MoS_2 heterostructure. *J. Mater. Chem. A* **2019**, *7*, 24557-24568.

[S12] Y. Wang, Y. Yang, D. Zhang, Y. Wang, X. Luo, X. Liu, J.-K. Kim, Y. Luo. Inter-overlapped MoS_2/C composites with large-interlayer-spacing for high-performance sodium-ion batteries. *Nanoscale Horiz.* **2020**, *5*, 1127-1135.

[S13] W. Zhang, H. Zhou, Z. Huang, S. Li, C. Wang, H. Li, Z. Yan, T. Hou, Y. Kuang. 3D hierarchical microspheres constructed by ultrathin MoS_2-C nanosheets as high-performance anode material for sodium-ion batteries. *J. Energy Chem.* **2020**, *49*, 307-315.

[S14] H. Lim, H. Kim, S.-O. Kima, W. Choi. Self-assembled N-doped MoS_2/carbon spheres by naturally occurring acid-catalyzed reaction for improved sodium-ion batteries. *Chem. Eng. J.* **2020**, *387*, 124144.